Boletim Técnico da Escola Politécnica da USP

Departamento de Engenharia Eletrônica

ISSN 1413-2206

BT/PEE/9701

Identification of Unstable Mechanical Systems

Roberto Moura Sales
Anselmo Bittar
Michael Porsch
Laércio Lucchesi

São Paulo - 1997

O presente trabalho é um resumo da dissertação de mestrado apresentada por Roberto Moura Sales, sob orientação dos Profs. Drs. Anselmo Bittar, Michael Porsch e Laércio Lucchesi: "Projeto de um Sistema de Controle para um Rotor Apoiado por Mancais Magnéticos", defendida em 19/12/96, na Escola Politécnica.

A íntegra da dissertação encontra-se à disposição com o autor e na Biblioteca de Engenharia de Eletricidade da Escola Politécnica/USP.

Sales, Roberto Moura
Identification of unstable mechanical systems / R.M. Sales, A. Bittar, M. Porsch, L. Lucchesi. -- São Paulo : EPUSP, 1997.
19p. -- (Boletim Técnico da Escola Politécnica da USP, Departamento de Engenharia Eletrônica, BT/PEE/9701)

1. Controle automático I. Bittar, Anselmo II. Lucchesi, Laércio III. Porsch, Michael IV. Universidade de São Paulo. Escola Politécnica. Departamento de Engenharia Eletrônica V. Título VI. Série
ISSN 1413-2206 CDD 629.8

Identification of Unstable Mechanical Systems

Roberto Moura Sales
Anselmo Bittar
Michael Porsch
Laércio Lucchesi

Depto. de Engenharia Eletrônica
Escola Politécnica da USP
Caixa Postal 61548 S.P. - CEP 05424-970
e-mail: roberto@lac.usp.br

Abstract

In this paper non-linear, unstable, SISO and MIMO mechanical systems are considered. Among three case studies, the first one consists of a lightly damped flexible beam hinged at one end and magnetically levitated at the other end; the second system consists of a magnetically supported rotor, which acts as a water pump in a water tunnel; the third system consists of a magnetically levitated vehicle prototype. Due to the unstable characteristic, several aspects related to closed loop experimental identification of each system are discussed. Analytical and/or experimental models are obtained for each system.

Introduction

Mechanical systems that use magnetic bearings are frequently employed in many situations related to rotating machines, robotics and more recently for levitated transport systems (Sinha, 1987). This paper is concerned with the identification of three unstable mechanical systems which employ magnetic bearings. The electromagnet systems adopted are inherently unstable, which introduces additional difficulties for any experiment.

The first system is the simplest one in the sense that it is inherently SISO. It consists of a lightly damped flexible beam hinged at one end and magnetically levitated at the other end. The second system consists of a magnetically supported rotor, which acts as a water pump in a water tunnel for hydrodynamic tests; the supporting system for the rotor avoids thus the introduction of turbulence in the water flow. In this case study, resonance frequencies are not relevant, and although it is a MIMO system, the identification procedure could be carried out as in the previous SISO case; the specific characteristics of the rotor resulted in a 5 input-5 output model, particularly suitable for the design of 5 independent controllers. Finally, the third system, a magnetically levitated vehicle prototype, is considered as an inherently MIMO system; in this case, resonance frequencies are present, and too high order models are obtained if some approximations are not taken into account. This system has 4 inputs and 4 outputs.

The paper is outlined as follows: firstly a brief description of each system is presented. The identification procedures and experimental results are then presented for each system. The last section contains general comments and conclusions.

Description of the Systems

Description of the Beam System

The flexible beam considered in this section constitutes a research set up developed for the investigation of different control design techniques when the resonance frequency of the system varies. A schematic diagram of this system is shown in Fig. 1.

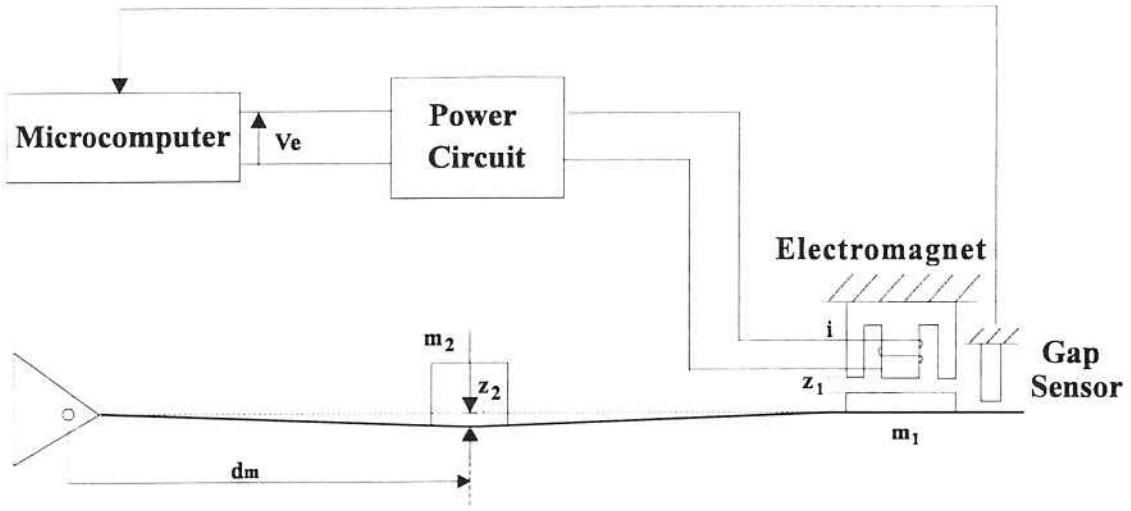

Figure 1: Schematic diagram of the magnetically levitated flexible beam.

In this figure, m_1 is a mass of steel through which the magnetic circuit of the electromagnet is closed. The mass m_2 represents a varying load in the middle of the beam, i represents the electrical current, z_1 and z_2 represent the gap of the electromagnet and the deflection of the beam, respectively. The movement of the beam is only in the vertical plane. In order to keep the beam levitated, the gap z_1 of the electromagnet must be controlled. The dimensions of the flexible beam are shown in Table 1.

Length	1.28 m
Width	5.08 cm
Thickness	6.35 mm

Table 1: Dimensions of the flexible beam

It is worth to mention some points on the choice of the steady state gap for the electromagnet. Figure 2 shows a schematic diagram of the designed electromagnet.

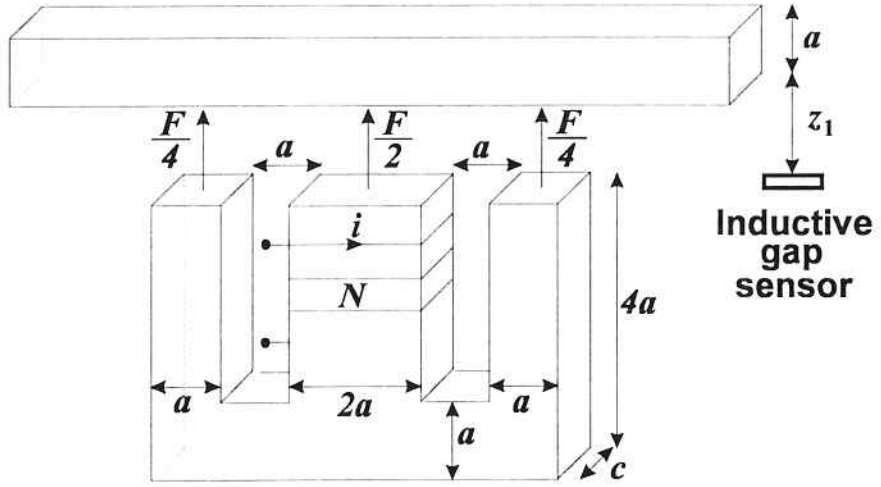

Figure 2: Electromagnet scheme.

For this type of electromagnet, the attraction force is given by:

$$F(t) = k_f \left(\frac{i(t)}{z_1(t)} \right)^2 \quad (1)$$

where:

i(t): input electrical current,

$z_1(t)$: output air gap,

$k_f = \frac{\mu_0 acN^2}{2}$: constant.

Loosely speaking, the choice of the steady state gap is directly related to the opposite requirements of energy consumption and levitation system robustness. In terms of energy consumption, it is interesting to set the gap as small as possible, in order to get smaller current intensity for levitation. However, for very small gaps, magnetic core saturation may occur, increasing the coil inductance, and leading thus to slow control action; hence, from the point of view of the levitation system robustness, higher gaps are more suitable. In this work, the nominal gap was set as Z_0 = 5mm. This choice is also function of the total mass of the system and electromagnet dimensions. In Table 2 some design data for the electromagnet are presented.

Nominal air gap	$Z_0 = 5$ mm
Steady state current	$I_0 = 0.7$ A
Dimensions	a = 3 cm c = 6 cm
Number of turns	N=1300
Air permeability	$\mu_0 = 4\pi 10^{-7}$ (H/m)

Table 2: Data for the electromagnet.

Description of the Rotor System

This section describes a magnetically supported rotor, which acts as a water pump in a closed circuit water tunnel. Figure 3 shows a schematic diagram of the rotor and its supporting bearings. The purpose of such system is to avoid vibrations through the water flow, which degrades the quality of hydrodynamic tests.

The rotor consists of a 60 cm diameter ring with the propeller in its center; the complete system mass is 75 Kg. The set up is mounted to operate in the vertical plane. The magnetic supporting system consists of 6 electromagnets to levitate and stabilize the ring in the radial plane (electromagnets 7 to 12), and 6 electromagnets to stabilize the rotor in the axial direction (electromagnets 1 to 6).

The electromagnets operate in pairs: 1 - 4, 2 - 5, 3 - 6 in the axial axis and 10 - 11 in the horizontal axis; the only exception is the vertical axis in which the electromagnets 7, 8 and 9 operate with the electromagnet 12, in order to compensate the gravity action. We have thus 5 points to be controlled; a position sensor is placed at each point.

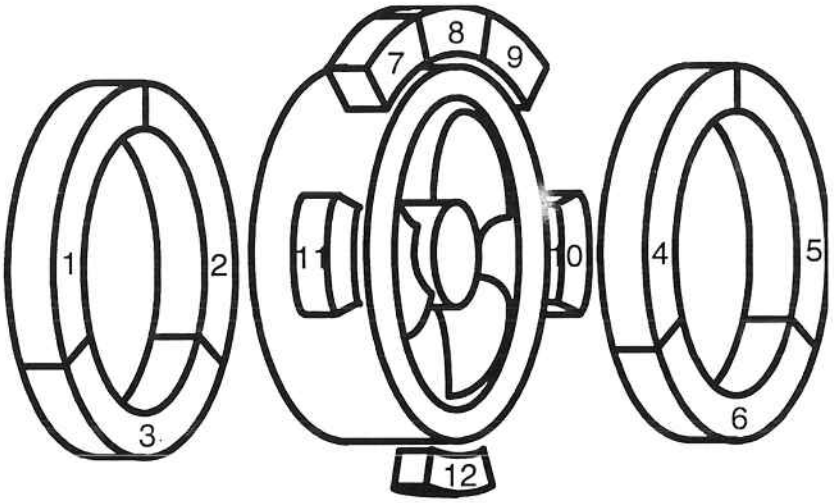

Figure 3: Schematic diagram of the rotor system

Description of the Vehicle System

The constructed system consists of a magnetically levitated vehicle prototype. The levitation is achieved by attraction forces developed by four electromagnets which were positioned in each extremity of the vehicle as shown in Fig. 4. There are also four gap sensors to measure the gaps of these electromagnets.

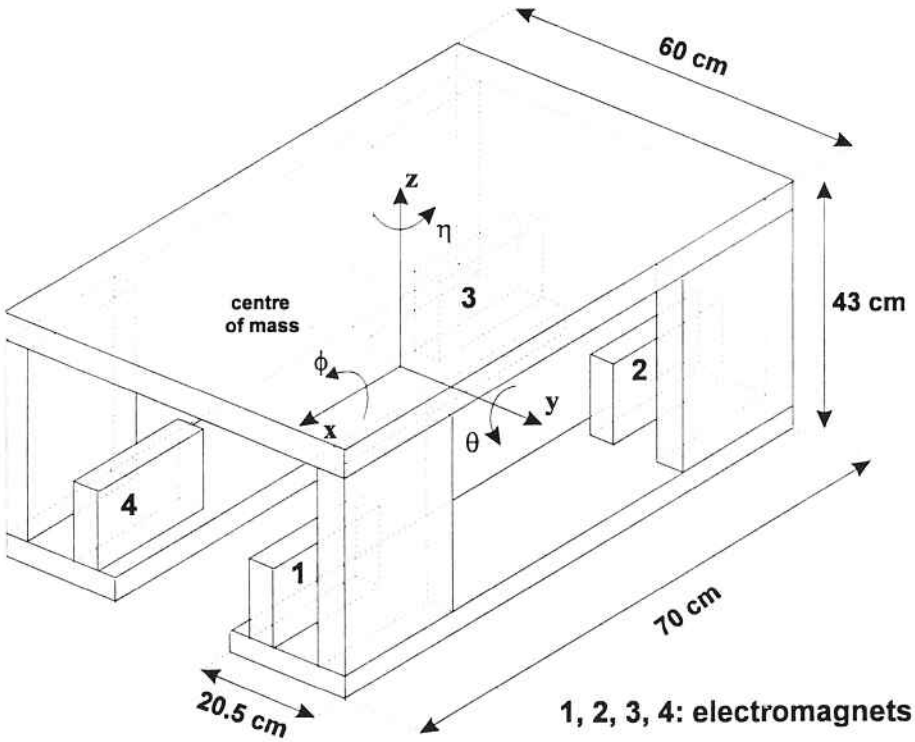

Figure 4: Schematic diagram of the vehicle prototype.

Since the magnetic forces in this case are always attraction forces, an elevated way was also constructed. A vehicle frontal view in levitation state is presented in Fig. 5. The vehicle levitation is achieved through the control of the gaps z_j, j = 1, 2, 3, 4.

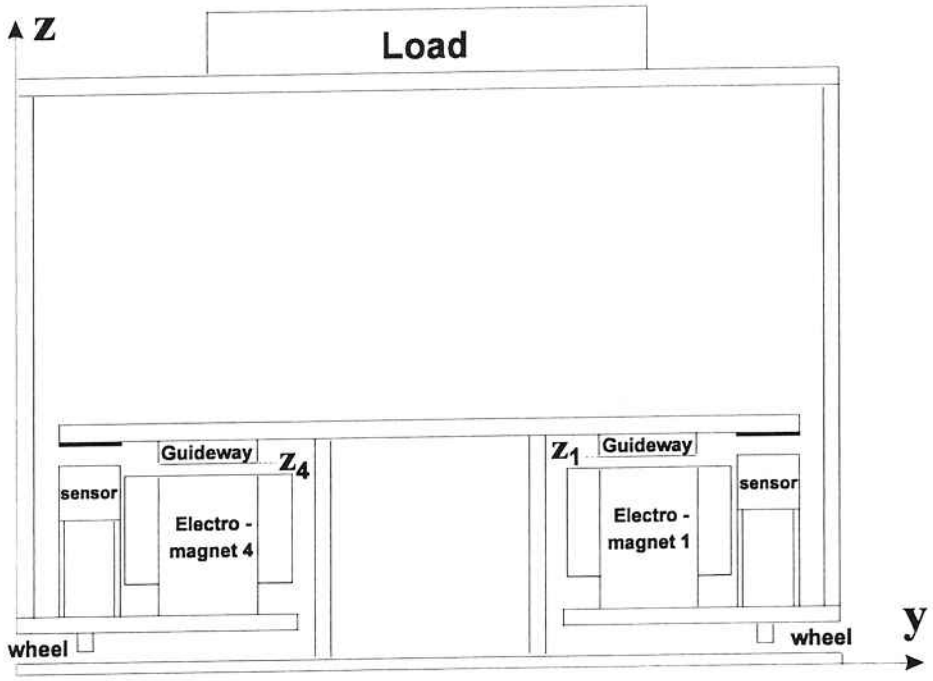

Figure 5: Vehicle frontal view.

The vehicle has six degrees of freedom which correspond to the three translation motions (x, y, z) and to the three rotation motions (ϕ, θ, η). The vehicle will have independent lift, guide and propulsion systems, but only the levitation system (control of z, ϕ and θ) has been considered in this paper. In order to control the guide system (y e η), it would be necessary to add four lateral electromagnets and to control the respective gaps.

The vehicle was constructed with aluminum plates. The guideways, through which the magnetic flux flows, were constructed with iron bars of small thickness. Laminated guideways would be an alternative choice in order to reduce eddy currents which produce drag and repulsive forces. Drag forces causes power loss and repulsive forces reduce the lift forces (Sinha, 1984). However, iron bars were employed in order to simulate such problems that will be certainly present in any real system. Table 3 presents some prototype data.

Length	70 cm
Width	60 cm
Height	43 cm
Mass	M_v=97.6 kg
Supply Voltage	55 V DC
Levitation power	377 W

Table 3: Prototype data.

Electromagnets for Levitation

The prototype studied in this work has independent electromagnets to lift and to guide the vehicle. This kind of construction provides controllers with simpler structures and improves the reliability

of the system (Sinha, 1984). The levitation electromagnets have an "E" shape as in the beam system (Fig. 2), and its design data are also those of Table 2, except the steady state current, I_0, which is equal to 1.71A.

Identification of the Systems

In this section identification procedures and results for each system described before are presented. The common characteristics of the three systems are the fact that they are non-linear and open loop unstable. On the other hand, they present particular features from the point of view of control design. As it will be seen, the flexible beam is an inherently SISO system; in spite of the fact that the rotor is a MIMO system, its particular mechanical characteristics allow the employment of 5 independent controllers, i.e., the plant behaves in fact as a set of SISO decoupled systems; finally, the vehicle prototype will be treated as a MIMO system. Although the unstable characteristic leads to similar identification experiments, the SISO/MIMO behavior imposes specific data treatment.

In the three cases the system to be identified includes the power circuit, the electromagnet, the plant and the sensor. Due to open loop instability, experimental models can be obtained only through closed loop experiments. The first step in the identification procedure was always the adjustment of simple SISO lead-lag controllers in order to stabilize the system. In the case of the beam, such preliminary design consists of the design of a single one input - one output controller; for the rotor and the vehicle 5 and 4 independent SISO controllers, respectively, have to be designed. Some details on the controller designs are presented in (Bittar, Sales, Lucchesi and Lima, 1995).

All the experiments are based on the injection of sinusoidal signals in the closed loop. An "HP 3562A Dynamic Signal Analyzer" was employed to inject the sinusoidal signal, and to compute the desired frequency responses as it will be described in the sequel. The noise presence was permanently monitored and for all practical considerations it could be disregarded.

Identification of the Beam System

In order to get some insight into the physics of this system, a simple mathematical model, which can be synthesized in two nonlinear equations relating the involved forces, is presented below - see (Fujita, Matsumura and Shimizu, 1990) for more details:

$$\begin{aligned} m\frac{d^2z_1}{dt^2} &= mg - k_f\left(\frac{i}{z_1}\right)^2 + \alpha(2\cdot z_2 - z_1) + \beta\frac{d}{dt}(2\cdot z_2 - z_1) \\ M_b\frac{d^2z_2}{dt^2} &= M_b g - 2\alpha(2\cdot z_2 - z_1) - 2\beta\frac{d}{dt}(2\cdot z_2 - z_1) \end{aligned} \qquad (2)$$

where

$$M_b = \frac{m_{beam}}{2} + m_2$$

$$m = \frac{m_{beam}}{2} + m_1$$

k_f - constant proportional to the air permitivity and dependent of the electromagnet dimensions,

α, β - constants that represent forces due to the deflection of the beam,

$k_f\left(\frac{i}{z_1}\right)^2$ - attraction force produced by the electromagnet,

i - electric current,

g - gravity.

The linearization of Eq.(2) produces, in addition to the resonant mode (poles in $\pm 80j$), two real poles (± 70), one stable and one unstable, as shown in Eq.(4). This transfer function includes also one stable pole in -250, which reflects the power circuit dynamic effects and the inductance of the electromagnet (Eq.3). It is assumed that:

$$\frac{I(s)}{V_e(s)} = \frac{k_b}{s+250} \tag{3}$$

where V_e is the input of the power circuit.

This term was estimated experimentally and incorporated in the final transfer function (Eq.4). Since many of the involved constants in Eq.(2) are not easily computed with precision, the obtained transfer function must be taken just as a rough approximation, which will be used for the first controller design.

$$\frac{Z_1(s)}{V_e(s)} = \frac{1690(s+76j)(s-76j)}{(s+250)(s+70)(s-70)(s+80j)(s-80j)} \tag{4}$$

The preliminary stabilizing controller allows to go on the experiments. In this case, the block diagram that represents the stabilized closed loop system for the identification experiments is shown in Fig. 6.

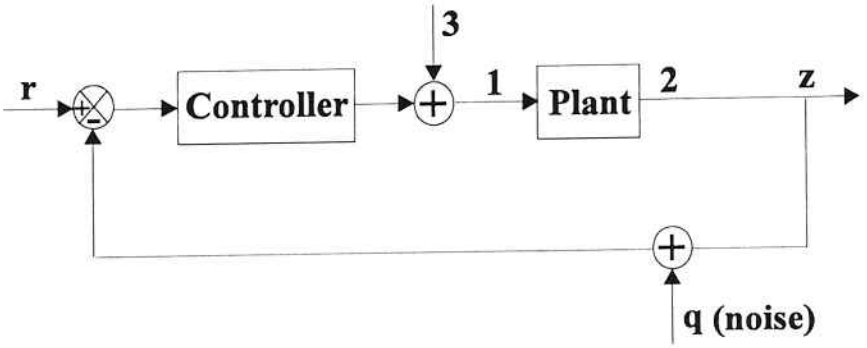

Figure 6: Closed loop block diagram.

Sinusoidal signals of suitable frequencies are injected in point 3. The signals in points 1 and 2 are then measured and their Fourier transforms computed, resulting thus the corresponding frequency response. The injected frequency signal ranges from 10^{-1} Hz to 10^{2} Hz.

It is assumed that m_2 may vary in its position and mass; this assumption leads to specific difficulties since it produces changes in the resonance frequencies. As control specification, it is considered that only the first resonance frequency should be "controlled", in the sense that it will be the only one included in the controller bandwidth; in addition, the controller should stabilize robustly the plant. These facts have direct implications in the final identified mathematical model.

After measurements are taken, the magnitude and phase plots of $Z_1(jw)/V_e(jw)$ may be obtained. Nine situations are considered accordance to the position d_m and the value of the mass m_2, as shown in Table 4 (the entries of the table represent the model numbers associated to the measurements when the corresponding d_m and m_2 are considered). Thus, as an example, model number 5 corresponds to m_2=1.50kg and d_m=0.71m.

d_m(m) / m_2 (kg)	0.565	0.710	0.850
1.25	1	2	3
1.50	4	5	6
1.75	7	8	9

Table 4: Variations of m_2 and d_m

Then, for each data set a curve fit was carried out. In order to fit suitably all data set, a transfer function with 16 zeros and 17 poles was adopted, resulting thus 9 transfer functions. Table (5) presents the poles and zeros of the model number 5.

Zeros (Hz)	**Poles (Hz)**
−72.50080	-1.55922
+6.99363	-1.29456
$-0.02875 \pm 5.38535 \cdot j$	+8.47039
$+0.02845 \pm 34.23650 \cdot j$	$-0.05321 \pm 6.02771 \cdot j$
$+0.55359 \pm 57.12440. j$	$-0.19195 \pm 34.01600 \cdot j$
$-1.26296 \pm 65.78970 \cdot j$	$-1.41261 \pm 65.62790 \cdot j$
$-0.16784 \pm 94.87340 \cdot j$	$-0.15000 \pm 94.83800 \cdot j$
$+0.13702 \pm 99.90610 \cdot j$	$-0.65930 \pm 54.18950 \cdot j$
$-33.82840 \pm 102.46800 \cdot j$	$+0.14164 \pm 99.88560 \cdot j$
Gain = -1.09	$-25.22210 \pm 117.55200 \cdot j$

Table 5: Poles and zeros of the model number 5.

A simple validation procedure for each transfer function can be obtained through the computation of the controller $K_{meas}(jw)$:

$$K_{meas}(jw) = \frac{G_{meas}(jw) - T_{meas}(jw)}{T_{meas}(jw) G_{meas}(jw)} \tag{5}$$

where $G_{meas}(jw)$represents the measured open loop frequency response from point 1 to point 2, and $T_{meas}(jw)$ represents the measured closed loop frequency response. The designed controller K(jw), which is obviously known, should be equal to $K_{meas}(jw)$ computed from Eq.(5). Figure (7) shows this comparison for the model number 5. The differences are due to difficulties to measure precisely the resonance frequencies (5Hz, 30Hz and 55 Hz, approximately).

The model number 5 (m_2=1.5kg and d=0.710m), for which the values of "d_m" and "m_2" correspond to central values for the admissible variations, was adopted as the nominal one. According to the control specifications, the controller should be robust for variations as in Table (4). Clearly, the order of the fitted nominal transfer function is too high (16 zeros and 17 poles) for control purposes. With this fact in mind, a model reduction algorithm was applied to this nominal transfer function.

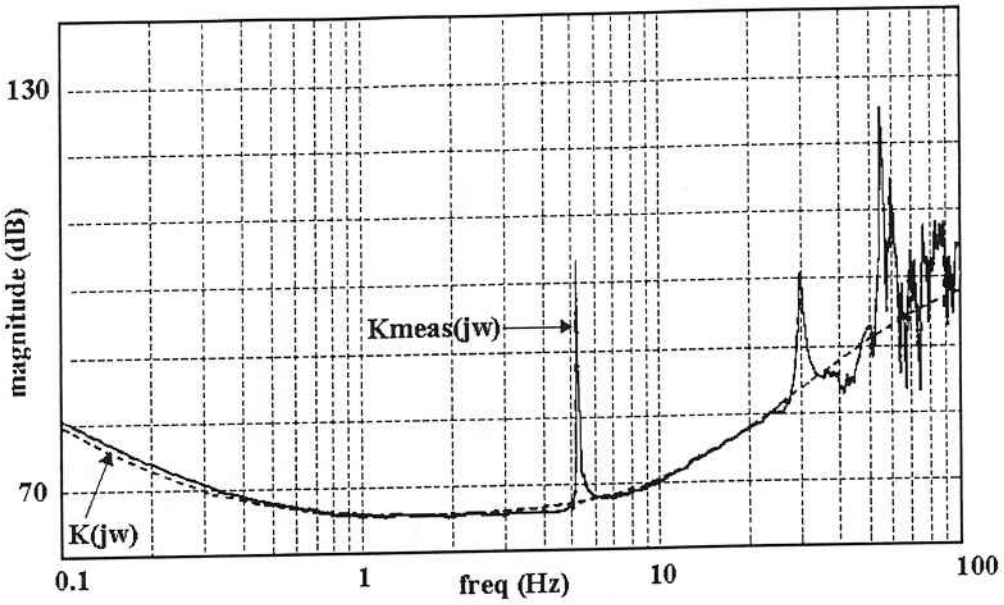

Figure 7: Comparison between $K_{meas}(jw)$ and K(jw).

Firstly, it can be observed that if it is desired that the model represents 3 resonance frequencies, then the least necessary degree for the denominator of the transfer function is 9, six of them representing the resonances. Similarly, if it is desired to model 2 resonance frequencies the least degree is 7, and to model 1 resonance frequency the least degree is 5. A mathematical model of order 3 is not able to represent any resonance frequency. Although this model of order 3 represents just the rigid mode of the beam and the electromagnet dynamic, it was chosen for control design. In order to justify this result, let's focus our attention on the modeling uncertainties, by computing the quantities:

$$|\Delta_A(jw)| = |G(jw) - G_N(jw)|$$

and

$$|\Delta_M(jw)| = \left|\frac{G(jw) - G_N(jw)}{G_N(jw)}\right|$$

where

$\Delta_A(jw)$ and $\Delta_M(jw)$ represent additive and multiplicative uncertainties, respectively;

G_N (jw) represents the nominal model after order reduction to 3 poles, (Fig.8), and 5 poles, (Fig.9);

G(jw) represents each one of the models (1, 2, 3, 4, 6, 7, 8, 9 in Table 4) of order 17.

Thus, from Table (4) the respective uncertainties are obtained:

- 8 uncertainty curves of the type $|\Delta_A(jw)|$ with respect to G_N(jw) of order 3;
- 8 uncertainty curves of the type $|\Delta_A(jw)|$ with respect to G_N(jw) of order 5;
- 8 uncertainty curves of the type $|\Delta_M(jw)|$ with respect to G_N(jw) of order 3;
- 8 uncertainty curves of the type $|\Delta_M(jw)|$ with respect to G_N(jw) of order 5.

In Figs. (8) and (9) some of these plots are shown.

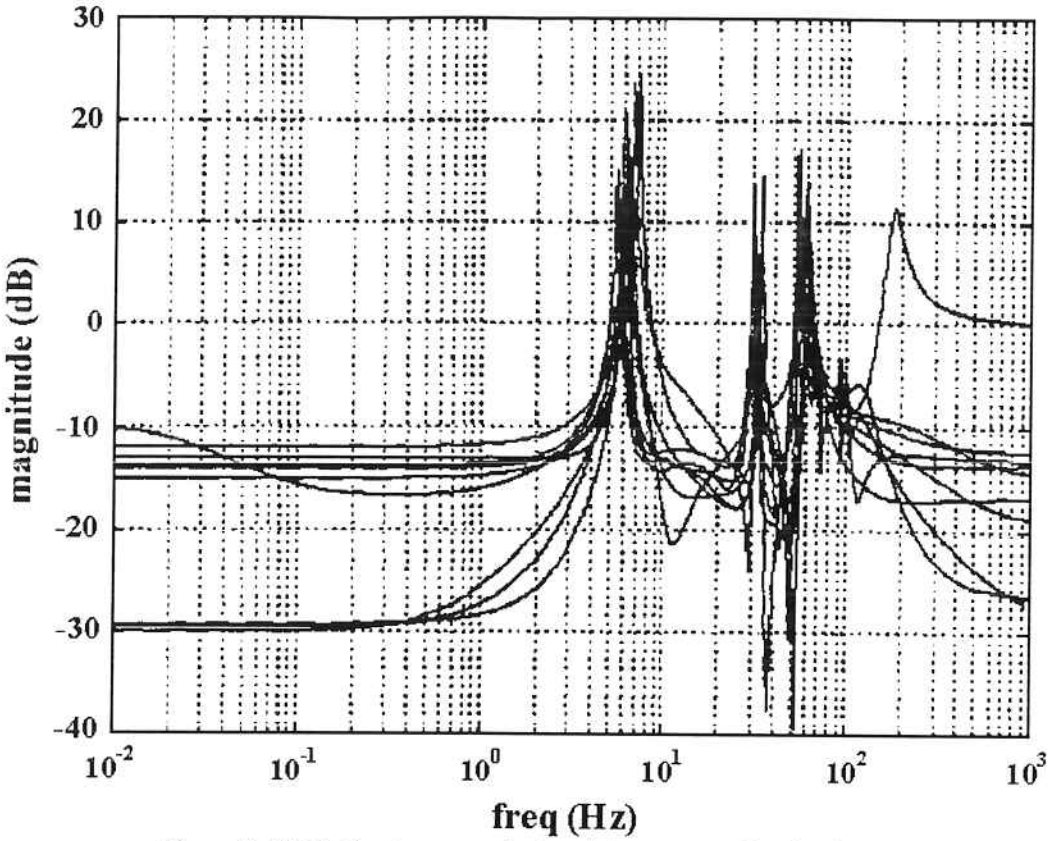

Figure 8: Multiplicative uncertainties with respect to G_N of order 3.

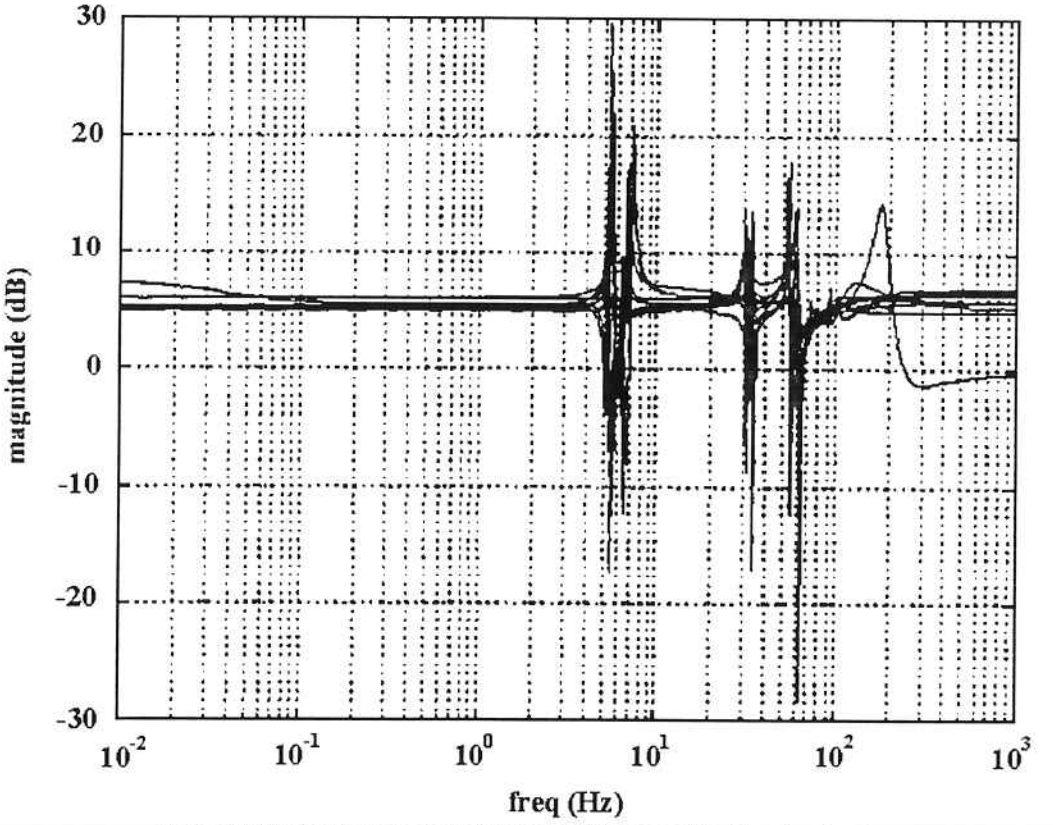

Figure 9: Multiplicative uncertainties with respect to G_N of order 5.

It is interesting to note that the superior contour for the uncertainty curves are very similar in both figures, above 5 Hz (similar results were obtained from the additive uncertainty plots). This is a consequence of the resonance frequency variation when m_2 and d_m vary. Hence, from the point of view of uncertainty modeling both transfer functions, of order 5 and 3, are equivalent. For simplicity the third order model is recommended for future control design. Equations (6) and (7) present below the transfer functions of order 5 and 3, respectively.

$$G_N(s) = \frac{-7.19(s-408.56)(s+412.90)(s-0.18\pm 33.83j)}{(s+97.97)(s+81.340)(s-53.22)(s+3.34\pm 37.87j)} \tag{6}$$

and

$$G_N(s) = \frac{-7.19(s-408.56)(s+412.90)}{(s+107.77)(s+89.47)(s-53.22)} \tag{7}$$

Identification of the Rotor System

For each pair of electromagnets a simple mathematical model can be derived from the schematic diagram of Fig. (10), where a pair of electromagnets applies forces F+ and F- to the mass, M_r, placed between them.

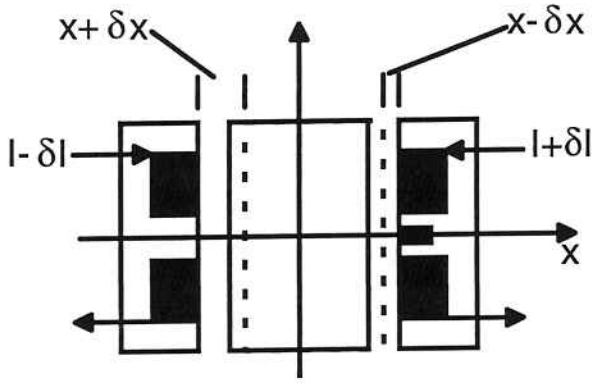

Figure 10: A pair of electromagnets.

In this case,

$$F_+ = K_m \frac{(I+\delta I)^2}{(x-\delta x)^2}$$

$$F_- = K_m \frac{(I-\delta I)^2}{(I+\delta I)^2}$$

and

$$F_r \overset{\Delta}{=} M_r \cdot \delta\ddot{x} = F_+ - F_- = K_m\left[\frac{(I+\delta I)^2}{(x-\delta x)^2} - \frac{(I-\delta I)^2}{(x+\delta x)^2}\right]$$

The state space nonlinear equations result as:

$$\overset{\Delta}{x_1} = \delta x$$

$$\dot{x}_1 = x_2$$

$$\dot{x}_2 = \frac{K_m}{M_r}\left[\frac{(I+\delta I)^2}{(x-\delta x)^2} - \frac{(I-\delta I)^2}{(x+\delta x)^2}\right]$$

and the linearized corresponding equations present two eigenvalues:

$$\lambda_{1,2} = \pm I\sqrt{\frac{K_m}{M_r x^3}}$$

similar to the beam case.

Following this procedure, the complete model was derived by considering each pair of electromagnet independently. In fact, the mechanical characteristics of the rotor suggested that there should have weak couplings between distinct pairs of electromagnets; this was experimentally confirmed as it will be seen in the sequel.

The parameter values for the rotor system are presented in Table (6).

M_r	75 kg
K_a (D, E and I electromagnets constants)	$1.5\text{x}10^{-4}$ Nm/A^2
K_r (X and Y axis electromagnets constants)	$1.78\text{x}10^{-4}$ Nm^2/A^2
Gap	0,015 mm

Table 6: Parameter Values for the Rotor System

The linear dynamic equations, in the case of the horizontal axis, are:

$$\begin{bmatrix}\dot{x}_1\\ \dot{x}_2\end{bmatrix} = \begin{bmatrix}0 & 1\\ 2.8\cdot 10^3 & 0\end{bmatrix}\cdot\begin{bmatrix}x_1\\ x_2\end{bmatrix} + \begin{bmatrix}0\\ 4.2\end{bmatrix}\cdot u$$

$$y = \begin{bmatrix}0.2\cdot 10^3 & 0\end{bmatrix}\cdot\begin{bmatrix}x_1\\ x_2\end{bmatrix} \qquad (8)$$

where $x_1 = \delta x$, $x_2 = \delta\dot{x}$, $u = \delta I$, and the output matrix represents the position sensor gain (V/m). The equilibrium point is around I = 1 A.

As in the analytical modeling, the experimental measurements were taken independently for each bearing pair. In this case, the experimental procedure follows exactly that one of the beam system.

From Fig. (9) it can be noted that the experimental measurements are close to the analytical model (Eq.8), confirming so the weak couplings in the system. Note that, differently from the beam case, the power circuit and the inductance dynamic effects were neglected in Eq. (8), without introducing significant errors.

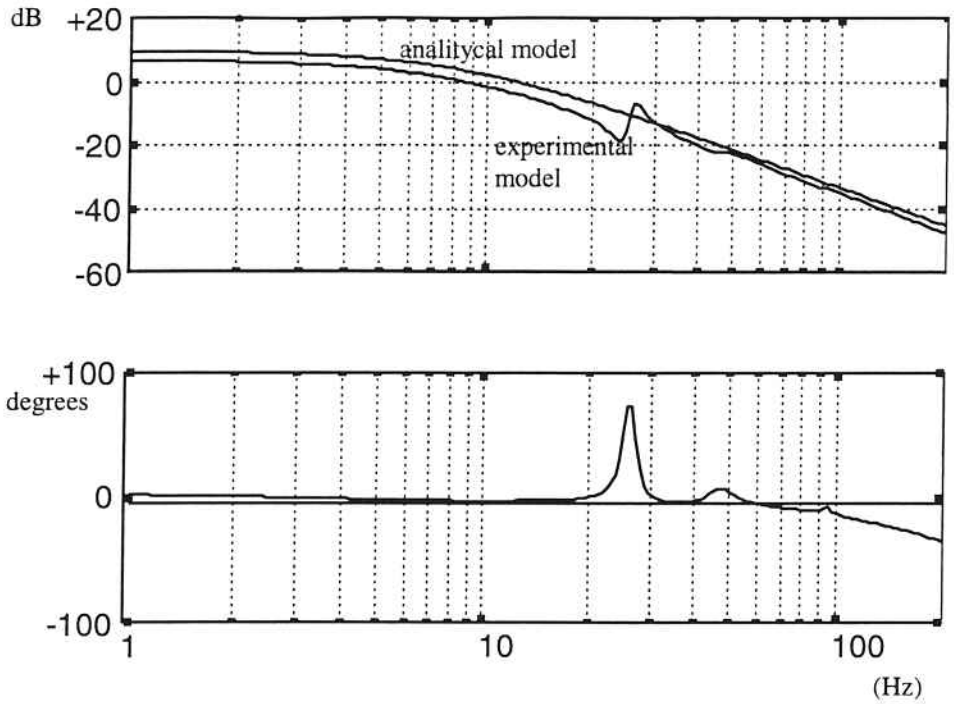

Figure 11: Horizontal axis Bode plots for the analytical and experimental models

Identification of the Vehicle

Although an analytical model could be developed as in (Jayawant, Sinha, Wheeler, Whorlow and Willsher, 1976), in this section only the experimental identification procedure and the corresponding results for the vehicle prototype are presented. The point that makes this case different from the above considered systems is the multivariable characteristic. As it will be seen, this fact may lead to very high order models, and some special care must be taken.

As in the rotor case, the first step consists in the design of four independent stabilizing controllers $k_iG_c(s)$ (i=1, 2, 3, 4), implemented as in Fig. (12).

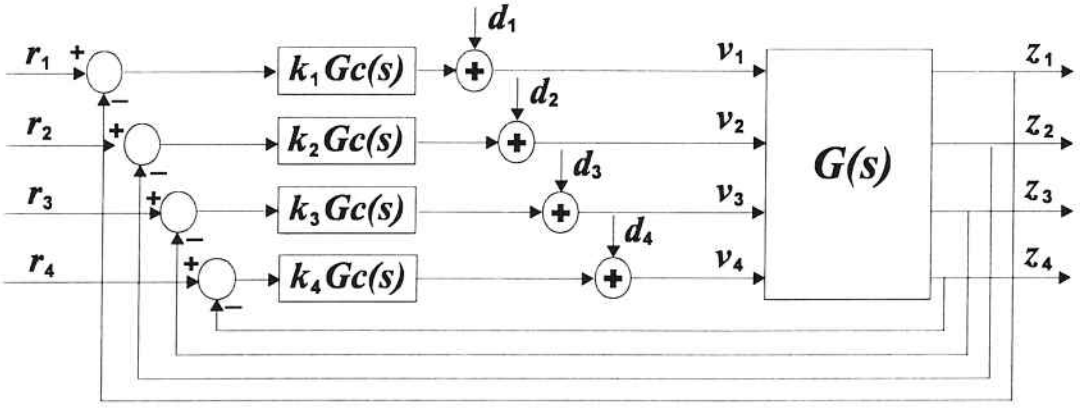

Figure 12: System block diagram.

The second step consists in the measurement of the closed loop frequency response. A sinusoidal signal, d_1, is injected as in Fig. (12) and the 4 system outputs, z_1, z_2, z_3 and z_4, are acquired. The same procedure is repeated separately for the remaining inputs d_2, d_3 and d_4, and thus 16 closed loop frequency responses are obtained.

The same number of inputs and outputs allows some simple operations in order to get an experimental model, i.e.:

$$z_m(jw) \stackrel{\Delta}{=} (I + G(jw)K(jw))^{-1} G(jw)d(jw) \tag{9}$$

or

$$z_m(jw) \stackrel{\Delta}{=} G_{mf}(jw)d(jw) \tag{10}$$

and hence

$$G(jw) = G_{mf}(jw)(I - K(jw)G_{mf}(jw))^{-1} \tag{11}$$

for every w such that $(I - K(jw)G_{mf}(j\,w))$ is invertible,

In the above equations $K(jw) = G_c(jw)\ \mathrm{diag}(k_1\ k_2\ k_3\ k_4)$, k_i $(i = 1, 2, 3, 4)$ constant, and

$$d(jw) \stackrel{\Delta}{=} \begin{bmatrix} d_1(jw) \\ d_2(jw) \\ d_3(jw) \\ d_4(jw) \end{bmatrix} \qquad z_m(jw) \stackrel{\Delta}{=} \begin{bmatrix} z_1(jw) \\ z_2(jw) \\ z_3(jw) \\ z_4(jw) \end{bmatrix}$$

Clearly, the computation of Eq. (11) can be easily performed in the numerical case, i.e., the gain and the phase of G(jw) can be computed for each w. On the other hand, if a curve fit is performed for each experimental frequency response in $G_{mf}(jw)$, then an analytical expression can be obtained for G(jw). However, in this last case too long expressions may occur. This fact can be illustrated for a system with the same number of inputs and outputs, as follows. Let:

ℓ : number of inputs or outputs of the system;

ρ: degree of the denominator of $G_c(s)$;

σ: degree of the common denominator of $G_{mf}(s)$;

$G(jw) \stackrel{\Delta}{=} G_n(jw)$: open loop frequency response computed numerically through Eq. (11);

$G(s) \stackrel{\Delta}{=} G_a(s)$: open loop transfer function matrix computed analytically through Eq. (11).

If there is not any zero-pole cancellation, the common denominator degree, ν, of the transfer function matrix $G_a(s)$ is given by:

$$\nu = (\rho + \sigma)\ell$$

In this case, the minimal state space realization (Kailath, 1980) for $G_a(s)$ is given by the McMillan degree, γ, which in the considered problem results as:

$$\gamma = \ell\nu = (\rho + \sigma)\ell^2 \tag{12}$$

Using a controller Gc(s) with ρ=6, Eq.(12) results as:

$$\gamma = (6 + \sigma) \cdot 4^2 = 96 + 16 \cdot \sigma \tag{13}$$

Equation (13) shows that even for small values of σ, the number of open loop states results high, which leads naturally to the application of order reduction algorithms. On the other hand, mechanical models with resonances are frequently ill conditioned, and under these conditions convergence of order reduction algorithms may fail. Fortunately, as a consequence of the geometrical and mechanical

symmetries of the vehicle, the 16 identified closed loop frequency responses are very similar; this allowed the approximation shown in the sequel.

In this sense, each one of the 16 closed loop frequency responses were approximated by the same transfer function with degree 4, producing a transfer function matrix $G_{mf}(s)$ with common denominator with degree 4 (σ=4). Figure (14) shows a typical frequency response, which relates the input d_1 to the output z_1, $G_{mf11}(s)$, for the experimental identification and for the adjusted transfer function with degree 4. The rigid body movement of the vehicle in 12rad/s was the main characteristic which was taken into account in this approximation. This curve fit produces, thus, an open loop model, $G_a(s)$, with 160 states (see Eq. 13).

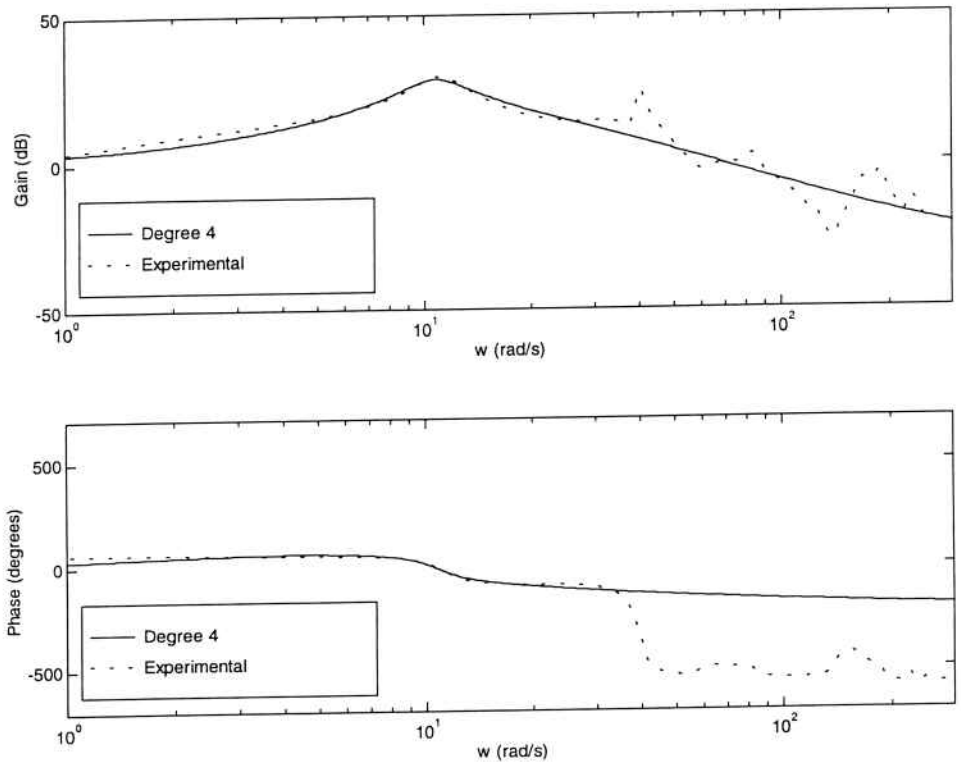

Figure 13: Frequency responses of $G_{mf11}(jw)$ for the experimental identification and for the approximated transfer function with degree 4.

Using Eq. (11), the computation of the numerical model $G_n(jw)$ and of the analytical model $G_a(s)$ produced the singular values presented in Fig. (14). In order to validate the model G_a (s) with 160 states, step disturbances d_1, d_2, d_3 and d_4 were applied simultaneously to the real and simulated closed loop system. Fig. (15) shows the corresponding time responses.

Although the results in Figs. (14) and (15) may be satisfactory, the identified model $G_a(s)$ with 160 states is considered a high order model for control design, for example. An order reduction algorithm, based on Schur method, was then applied. It is worth to mention that many algorithms were tested, and that due to numerical problems, convergence was achieved only when the state space equations were written using Gilbert's realization (Kailath, 1980). The model of 160 states, $G_a(s)$, was, thus, reduced to a model of 16 states. The singular values for the complete and the reduced order model resulted very similar, as shown in Fig. (16).

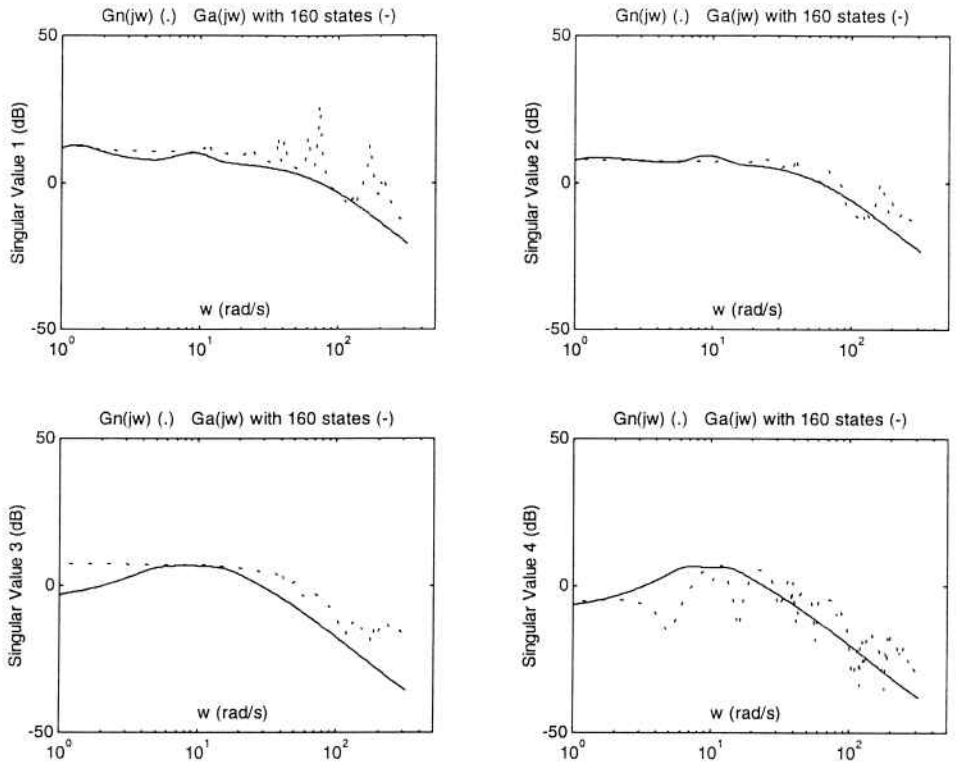

Figure 14: Singular values of $G_n(jw)$ and $G_a(jw)$.

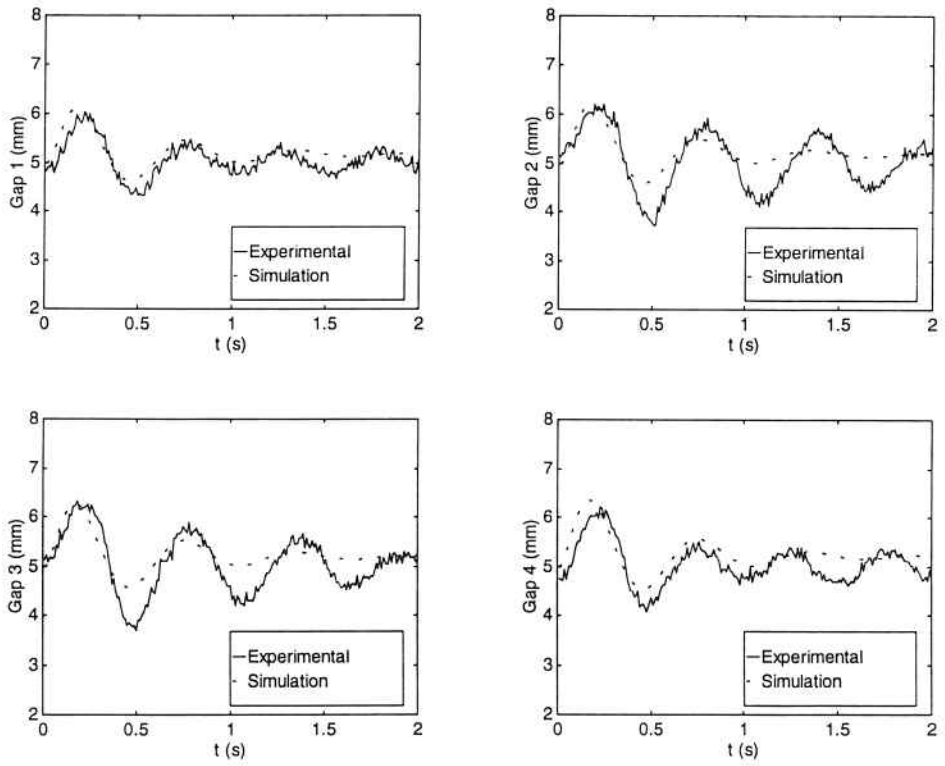

Figure 15: Closed loop system response for a step disturbance applied in plant inputs.

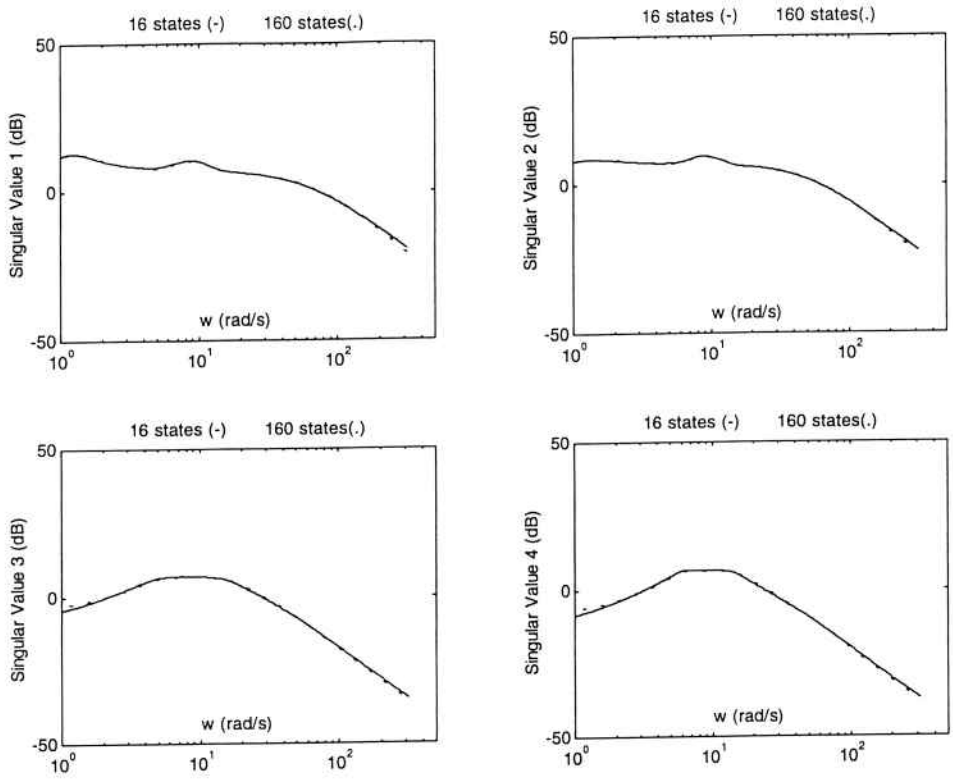

Figure 16: Singular values of the model $G_a(jw)$ with 16 and 160 states.

Equations (14) and (15) present the identified closed loop transfer function matrix, $G_{mf}(s)$, with common denominator of degree 4 and the controller transfer function matrix, K(s), respectively.

$$G_{mf}(s) = -\begin{bmatrix} 1.000 & 0.308 & 0.395 & 1.259 \\ 0.218 & 1.665 & 1.004 & 0.285 \\ 0.390 & 1.191 & 1.221 & 0.549 \\ 0.916 & 0.391 & 0.374 & 1.894 \end{bmatrix} \cdot \frac{0.0256(s+1.6285)(s+10.2255)(s-248.5757)(s+683.0728)}{(s+2.0718\pm 10.5878j)(s+22.0294\pm 2.6509j)} \tag{14}$$

$$K(s) = -\begin{bmatrix} 0.2775 & 0 & 0 & 0 \\ 0 & 0.2667 & 0 & 0 \\ 0 & 0 & 0.2503 & 0 \\ 0 & 0 & 0 & 0.2394 \end{bmatrix} \cdot \frac{(s+0.84)(s+103.27)(s+126.21)(s\pm 7000.00)(s+7834.97)}{s(s+368.42)(s+340.30\pm 178.65j)(s+7196.12\pm 347.33j)} \tag{15}$$

Control Design and Implementation Considerations

In this section some brief comments on control design and implementation are presented. As observed in the "Identification of the Systems" section, the first step in the identification procedure was the adjustment of simple SISO lead-lag controllers to stabilize the plant. For the beam and the vehicle

systems, digital controllers to run a sampling frequency of 3 kHz were employed; the rotor controller was analogic.

The final model obtained for the flexible beam was used for H_2, H_∞ and H_2/H_∞ controller design purposes. The main results are presented in (Bittar, Sales, Lucchesi and Lima, 1995). The final model obtained for the rotor was used for an analogic H_∞ controller design. The main results are presented in (Porsch, 1996). In the case of the vehicle prototype, the final MIMO system has been the subject of research of H_2 and H_∞ digital controller designs. Robustness and performance are the main characteristics to be investigated.

Concluding Remarks

In this paper identification case studies for non-linear unstable SISO and MIMO mechanical systems were considered. The unstable characteristic imposes that any identification experiment should be carried out in a closed loop configuration.

In the first case study, a flexible beam, emphasis was given to the modeling uncertainty characterization, and the final model, potentially for control design, consisted of a third order model. The system has one input and one output, and the conclusion followed as a direct consequence of the variation of the resonance frequency of the beam. An interesting point to be noted is that, although the resonance frequency is not modeled in the suggested model, such model is suitable for control design even if it is desired that the controller actuates in this frequency range. It seems that some other approach, e.g., μ-synthesis, should be used in order to take into account the effect of the varying resonance.

In the second case study, a magnetically supported rotor, a simple mathematical model was analytically derived. The simplicity of the model relies on the fact that couplings among bearings were neglected. The analytical model was compared with experimental frequency responses and very good results were obtained, confirming so the low coupling assumed.

In the third case study, a magnetically levitated vehicle prototype, an experimental model was obtained. Special emphasis was dedicated to the characterization of the multivariable behavior of the plant. The first experimental model resulted a high order one, and order reduction algorithms had to be employed. In order to get convergence of these algorithms, Gilbert's state space realization developed a decisive role due to ill numerical conditioning of the model. The final 16 states model was validated through its singular values and time responses.

Acknowledgments

This research was supported by FAPESP under grants 91/2344-8 and 95/6968-7.

References

Bittar, A., Sales, R. M., Lucchesi, L., Lima, A. C., 1995, "Some Design Difficulties and Control Results for a Magnetically Levitated Beam", Proceedings of the third European Control Conference, vol. 4, pp. 3498-3503.

Fujita, M., Matsumura, F., Shimizu, M., 1990, "H_∞ Robust control design for a magnetic suspension system", 2nd International Symposium on Magnetic Bearing , Tokyo, Japan, July 12-14.

Jayawant, B. V., Sinha, P. K., Wheeler, A. R., Whorlow, R. J., Willsher, J., 1976, "Development of 1-ton magnetically suspended vehicle using controlled d.c. electromagnets", Proceedings of the IEE, vol. 123, n°. 9, pp. 941-948.

Kailath, T., 1980, "Linear systems", N.J., Prentice-Hall Inc.

Porsch, M., 1996, "Projeto de Sistema de Controle para um Rotor Suportado Magneticamente", Dissertação de Mestrado, Departamento de Engenharia Eletrônica, Escola Politécnica da USP.

Sinha, P.K., 1984, "Design of a magnetically levitated vehicle", IEEE Transactions on Magnetics, vol. MAG-20, n°. 5, pp. 1672-1674.

Sinha, P. K., 1987, "Electromagnetic suspension: dynamics and control", London, Peter Peregrinus Ltd.

BOLETINS TÉCNICOS - TEXTOS PUBLICADOS

BT/PEE/9301 - Oscilador a HEMT - 10 GHz - FÁTIMA S. CORRERA, EDMAR CAMARGO
BT/PEE/9302 - Representação Senoidal da Voz através dos Polos do Filtro Preditor - MARCELO B. JOAQUIM, NORMONDS ALENS
BT/PEE/9303 - Blindagens por Grades Condutoras: Cálculo do Campo Próximo - LUIZ CEZAR TRINTINALIA, ANTONIO ROBERTO PANICALI
BT/PEE/9304 - Sistema de Otimização e Controle de Produção em Minas de Pequeno e Médio Porte - TSEN CHUNG KANG, VITOR MARQUES PINTO LEITE
BT/PEE/9401 - Determinação das Frases de Aplicação Forense para o projeto NESPER e Tese de Mestrado IME/94, com Base em Estudos Fonéticos - MARCONI DOS REIS BEZERRA, EUVALDO F. CABRAL JUNIOR
BT/PEE/9402 - Implementação e Teste de uma Rede Neural Artificial do Tipo KSON (Kohonen Self-Organizing Network) com Entradas Bidimensionais - MARCELO YASSUNORI MATUDA, EUVALDO F. CABRAL JR.
BT/PEE/9403 - Transformada de Walsh e Haar Aplicadas no Processamento de Voz - ALEXANDRE AUGUSTO OTTATI NOGUEIRA, THIAGO ANTONIO GRANDI DE TOLOSA, EUVALDO F. CABRAL JÚNIOR
BT/PEE/9404 - Aplicação de Redes Neurais ao Problema de Reconhecimento de Padrões por um Sonar Ativo - ALEXANDRE RIBEIRO MORRONE, CRISTINA COELHO DE ABREU, EDUARDO KOITI KIUKAWA, EUVALDO F. CABRAL JR.
BT/PEE/9405 - Tudo que se Precisa Saber sobre a Prática da FFT - Transformada Rápida de Fourier (Inclui Software) - ROGÉRIO CASAGRANDE, EUVALDO F. CABRAL JR.
BT/PEE/9406 - A Survey on Speech Enhancement Techniques of Interest to Speaker Recognition - CELSO S. KURASHIMA, EUVALDO F. CABRAL JR.
BT/PEE/9407 - Identificação de Pulsos Decádicos em Linhas Telefônicas - ANTONIO P. TIMOSZCZUK, MÁRCIO A. MATHIAS, EUVALDO F. CABRAL JR.
BT/PEE/9408 - Implementação e Teste de Filtros do Tipo Adaptativo e "Notch" para a Remoção de Interferência de 60 Hz em Sinais de Eletrocardiograma - FLÁVIO ANTÔNIO MENEGOLA, JOSÉ AUGUSTO DE MATTOS, JOSÉ GOMES G. FILHO, SIDNEY SILVA VIANA, EUVALDO F. CABRAL JR.
BT/PEE/9409 - Compressão de Sinais de Voz utilizando Transformadas de Karhunen-Loève, Fourier e Hadamard - IVAN LUIS VIEIRA, LUIZ FERNANDO STEIN WETZEL, EUVALDO F. CABRAL JR.
BT/PEE/9410 - "Ray Tracing" Paralelo - EDUARDO TOLEDO SANTOS, JOÃO ANTONIO ZUFFO
BT/PEE/9411 - Implementação de uma Ferramenta Posicionador para "Gate-Arrays" Tipo Mar de Portas - JORGE W. PERLAZA PRADO, WILHELMUS A. M. VAN NOIJE
BT/PEE/9412 - Tudo que se Precisa Saber Sobre a Teoria da FFT - Transformada Rápida de Fourier - FÁBIO LUÍS ROMÃO, REINALDO SILVEIRA, ROGÉRIO CASAGRANDE, EUVALDO CABRAL JR.
BT/PEE/9413 - Análise do Ruído Sonoro em uma Sala de Aquisição de Amostras de Som com Microcomputador - FÁBIO LUÍS ROMÃO, REINALDO SILVEIRA, EUVALDO CABRAL JR.
BT/PEE/9414 - Cor: Aspectos Relevantes para Visualização de Dados - SÍLVIA DELGADO OLABARRIAGA
BT/PEE/9415 - Projeto de Filtros Digitais IIR com Fase Aproximadamente Linear Utilizando Redução de Ordem - IVAN F. J. RODRIGUES, MAX GERKEN
BT/PEE/9416 - GERAFILTRO: Sistema para Projeto Automático de Filtros Digitais "IIR" (da especificação em alto nível ao leiaute do "ASIC") - RICARDO PIRES, JOSÉ VIEIRA DO VALE NETO
BT/PEE/9417 - Redes Neurais Artificiais Aplicadas à Identificação de Pulsos Decádicos em Linhas Telefônicas - ANTONIO P. TIMOSZCZUK, EUVALDO F. CABRAL JR.
BT/PEE/9501 - Estudo Comparativo de Métodos de Cálculo da Frequência Fundamental - MARCOS COSTA HUNOLD, EUVALDO F. CABRAL JR.
BT/PEE/9502 - Combinando Técnicas de Redes Neurais Artificiais e Informações de Excitação no Reconhecimento Automático do Locutor - ANDRÉ BORDIN MAGNI, EUVALDO F. CABRAL JR.
BT/PEE/9503 - Utilização de Redes Neurais Artificiais para Detecção e Identificação de Falhas em Circuitos - MÁRCIO YUKIO TERUYA, ROBERTO AMILTON BERNARDES SÓRIA, EUVALDO CABRAL JR.
BT/PEE/9504 - Uso de Redes Neurais Artiificiais no Reconhecimento de Locutores no Domínio Temporal - BENEDITO JOSÉ BARRETO FONSECA JÚNIOR, EUVALDO CABRAL JÚNIOR
BT/PEE/9505 - Projeto de Filtros Passivos e Ativos em Técnicas de Circuitos Integrados de Microondas - DAVID VIVEIROS JÚNIOR, DENISE CONSONNI
BT/PEE/9506 - Uma Análise de *Clustering* para as Frases de Projeto NESPER - RONALDO OLIVEIRA MESSINA, EUVALDO F. CABRAL JR.
BT/PEE/9507 - Controle com Estrutura Variável e Modos Deslizantes - Um Estudo para Aplicação em Controle Carga-frequência da Geração - JOSE PAULO F. GARCIA, JOCELYN FREITAS BENNATON
BT/PEE/9508 - Recuperação das Margens de Ganho e de Fase para Sistemas de Fase Não Mínima por Realimentação da Saída - MARCO H. TERRA, VITOR M. P. LEITE
BT/PEE/9509 - Sistema de Inspeção Óptica de Dispositivos Bi-Dimensionais - CASIMIRO DE ALMEIDA BARRETO, PEDRO LUÍS PRÓSPERO SANCHEZ
T/PEE/9510 - Sistema de Partículas Uma Poderosa Técnica de Animação em Computação Gráfica - RENATO CURTO RODRIGUES, JOÃO ANTÔNIO ZUFFO
BT/PEE/9511 - Efeito de Ruídos em Sinais de Voz Visualizados em Trajetórias Neurais de Kohonen - CELSO S. KURASHIMA, EUVALDO F. CABRAL JR.
BT/PEE/9601 - "Um Reconhecedor de Sinais Sonoros Utilizando LVQ" - ALEXANDRE TORNICE, EUVALDO CABRAL JR.
BT/PEE/9602 - "Coleção *Artificial Neural Networks*: Uma Visão Geral dos Sistemas Neurais Artificais de Stephen Grossberg" - CHIU HSIUNG HUANG
BT/PEE/9603 - "Reactively-Sputtered TiN Formation Using a RF Magnetron System"- SÉRGIO PAULO AMARAL OSÓRIO, LUIZ SÉRGIO ZASNICOFF
BT/PEE/9604 - Aspectos em Tradução de Linguagens Naturais Através de Redes Neurais Artificiais - CARLOS EDUARDO DANTAS DE MENEZES, EUVALDO F. CABRAL JR.
BT/PEE/9605 - Implementação de Blocos Passa-Tudo Utilizando Realimentação de Erro - SÉRGIO JOSÉ CARNEIRO LEÃO, MAX GERKEN
BT/PEE/9606 - Coleção `SANN group` Redes Neurais Artificiais: A Rede Neural de Sakoe - ANDRÉ BORDIN MAGNI, EUVALDO F. CABRAL JR.

BT/PEE/9607 - Coleção SANN group Redes Neurais Artificiais: A Rede Neural de Steinbuch - ROBERTO AMILTON BERNARDES SÓRIA, EUVALDO F. CABRAL JR.
BT/PEE/9608 - Desenvolvimento de uma Estrutura de Duplo Nível de Metal para a Confecção de Interconexões em Circuitos Integrados - JOSÉ AUGUSTO DE ALENCAR PEREIRA, LUIZ CARLOS MOLINA TORRES
BT/PEE/9609 - Determinação de Parâmetros de Processo para Fotomáscara "Balzers" Utilizando Gerador de Padrões - JORGE SEKI, MEGUMI SAITO
BT/PEE/9610 - Um Ambiente para Desenvolvimento de Sistemas Distribuídos - PEDRO F. ROSA, JOÃO A. ZUFFO
BT/PEE/9611 - Interpretações Teóricas do Funcionamento Cerebelar: Uma Revisão - MARCUS FRAGA VIEIRA, ANDRÉ FÁBIO KOHN
BT/PEE/9612 - Marcapasso Cardíaco Temporário Microcontrolado de Demanda e Baixo Consumo - FLAVIO ANTONIO MENEGOLA, JOSÉ CARLOS TEIXEIRA DE BARROS MORAES
BT/PEE/9613 - Um Sistema de Planejamento de Ação Baseado em Casos para uma Célula Flexível de Manufatura - RICARDO LUÍS DE FREITAS, MÁRCIO RILLO
BT/PEE/9614 - Aplicações do Boundary-Scan para o Teste de Módulos Multichip - ROBERTO C. COSSI JR., JOSÉ ROBERTO DE A. AMAZONAS
BT/PEE/9615 - A 2.488 Gb/s GaAs 1:4/1:16 Demultiplexer IC with Skip Circuit for Sonet STS-12/48 Systems - TAUFIK ABRÃO, FATIMA S. CORRERA
BT/PEE/9616 - Uma Contribuição para a Construção de Algoritmos em Projetos de Redes - ALLAN DE SOUZA, JOSÉ ROBERTO CASTILHO PIQUEIRA
BT/PEE/9617 - Análise Crítica dos Métodos de Medição do Intervalo QT do Eletrocardiograma - SÍDNEY DA SILVA VIANA, JOSÉ CARLOS TEIXEIRA DE BARROS MORAES
BT/PEE/9618 - Deposição e Caracterização de Filmes de SiO_2 Crescidos pela Técnica de PECVD a Baixa Temperatura - MARCO ALAYO CHÁVEZ, INÉS PEREYRA
BT/PEE/9619 - PARSTOOL: Uma Ferramenta de Auxílio à Simulação de Sistemas Paralelos - LI KUAN CHING, LIRIA MATSUMOTO SATO
BT/PEE/9620 - Análise de um Método de Otimização por Malha no Treinamento de Robôs - OLÍMPIO MURILO CAPELI, JOSÉ CARLOS T. B. MORAES, SADAO ISOTANI